

Comparison of two superconducting phases induced by a magnetic field in UTe_2

W. Knafo,^{1*} M. Nardone,¹ M. Valiska,² A. Zitouni,¹ G. Lapertot,² D. Aoki,^{2,3} G. Knebel,² D. Braithwaite²

¹ *Laboratoire National des Champs Magnétiques Intenses, UPR 3228, CNRS-UPS-INSA-UGA, 143 Avenue de Rangueil, 31400 Toulouse, France*

² *Univ. Grenoble Alpes and CEA, IRIG-PHELIQS, F-38000 Grenoble, France*

³ *Institute for Materials Research, Tohoku University, Ibaraki 311-1313, Japan*

* *Corresponding author: william.knafo@lncmi.cnrs.fr*

29/06/2020 10:59

Abstract

Superconductivity induced by a magnetic field near metamagnetism is a striking manifestation of magnetically-mediated superconducting pairing. After being observed in itinerant ferromagnets, this phenomenon was recently reported in the orthorhombic paramagnet UTe_2 . Under a magnetic field applied along the hard magnetization axis \mathbf{b} , superconductivity is reinforced on approaching metamagnetism at $\mu_0 H_m \approx 35$ T, but it abruptly disappears beyond H_m . On the contrary, field-induced superconductivity was reported beyond $\mu_0 H_m \approx 40$ -50 T in a magnetic field tilted by ≈ 25 -30° from \mathbf{b} in the (\mathbf{b}, \mathbf{c}) plane. Here we explore the phase diagram of UTe_2 under these two magnetic-field directions. Zero-resistance measurements permit to confirm unambiguously that superconductivity is established beyond H_m in the tilted-field direction. While superconductivity is locked exactly at fields either smaller (for a $\mathbf{H} \parallel \mathbf{b}$), or larger (for \mathbf{H} tilted by $\approx 27^\circ$ from \mathbf{b} to \mathbf{c}), than H_m , the variations of the Fermi-liquid coefficient in the electrical resistivity and of the residual resistivity are surprisingly similar for the two field directions. The resemblance of the normal states for the two field directions puts constraints for theoretical models of superconductivity and implies that some subtle ingredients must be in play.

Unconventional superconductivity is observed in an ever-growing number of correlated electron systems [1], ranging from heavy-fermion [2,3], high-temperature cuprate [4], iron-based pnictide and chalcogenide [5], to the newly-discovered nickelate [6] and graphene-superlattice [7] families. New unusual superconducting phases continue to be discovered, such as those reported during the last two decades in the ferromagnets UGe₂, URhGe, and UCoGe [8,9,10]. Instead of antiferromagnetic fluctuations, which are suspected to play a role in most heavy-fermion superconductors [3], ferromagnetic fluctuations were proposed to drive the pairing mechanism of these materials close to a ferromagnetic quantum instability. In these three systems, a magnetic field also leads to a re-entrance or reinforcement of superconductivity, and magnetic-field-induced ferromagnetic fluctuations are suspected to directly control the pairing strength, which can be qualitatively understood as the enhancement of a ‘strong-coupling’ superconducting parameter λ with field [11].

In UGe₂ under pressure, a magnetic field along the easy magnetization axis **a** leads to a metamagnetic transition between two ferromagnetic phases, in the vicinity of which superconductivity is reinforced, as indicated by a S-shape in the temperature dependence of the superconducting critical field H_{c2} [12]. Reentrance or reinforcement of superconductivity occurs in the isostructural orthorhombic ferromagnets URhGe and UCoGe under a magnetic field applied along their hard magnetic axis **b** [13,14]. In URhGe, field-induced superconductivity coincides with a metamagnetic transition at $\mu_0 H_m = 12$ T, where enhanced magnetic fluctuations [15,16] accompany a sudden rotation of the magnetic moments (from the initial easy direction **c** to the direction **b**) [13]. The Curie temperature vanishes at H_m in a magnetic field **H** \parallel **b**, and a ‘wing structure’ of the ferromagnetic phase boundary, linked with a quantum critical end point, can be observed in a magnetic field tilted away from **b** [13]. In this system, as in other heavy-fermion materials, a Fermi surface instability is observed at H_m , beyond which a polarized paramagnetic (PPM) regime is established [17,18,19]. In UCoGe, a magnetic field along **b** leads to a reinforcement of superconductivity, which is also associated with the suppression of the Curie temperature at $\simeq 15$ T [14]. However, a metamagnetic transition occurs at a much higher field $\mu_0 H_m \simeq 50$ T, in relation with the temperature T_χ^{max} at which the magnetic susceptibility presents a broad maximum [20]. The strong exchange field in these ferromagnets indicates that a spin-triplet superconducting order parameter with equal-spin pairing may be realized [11], in contrast to most unconventional superconductors, where antiferromagnetic fluctuations are suspected to be the ‘glue’ for superconductivity and lead to a singlet order parameter. NMR experiments brought microscopic support for such triplet state and they further highlighted the role of magnetic fluctuations [21,22].

Recently, superconductivity was found to develop in the paramagnetic heavy-fermion material UTe₂ at temperatures below $T_{sc} = 1.6$ K [23,24]. This system crystallizes in an orthorhombic crystal structure with space group *Immm* (#71, D_{2h}^{25}) and it is characterized by an anisotropic magnetic susceptibility [see Figure 1(a)]. For a magnetic field applied along the easy magnetic axis **a**, a large low-temperature magnetic susceptibility and a scaling plot of magnetization data were interpreted as the indication for a nearby ferromagnetic instability [23]. However, no sign of ferromagnetic order has been found down to the lowest temperatures (25 mK) [25]. While magnetic fluctuations were observed by NMR [26] and muon-spin relaxation measurements [25], the ferromagnetic and/or antiferromagnetic nature of these fluctuations was not determined so far. By analogy with the above-mentioned ferromagnetic superconductors, a spin-triplet nature of superconductivity has been proposed for UTe₂ [23]. This proposition was made following the observation of i) a large anisotropic upper critical field which exceeds the normal paramagnetic limitation for all field directions [23,24], ii) a tiny change in the NMR Knight shift through T_{sc} [27], and iii) chiral edge

states possibly identified in the superconducting gap by STM experiments [28]. A magnetic field applied along the hard-magnetic axis \mathbf{b} induces a first-order metamagnetic transition at $\mu_0 H_m \approx 35$ T, which separates a low-field correlated paramagnetic (CPM) regime from a polarized paramagnetic regime [29,30,31]. It is accompanied by sudden jumps $\Delta M \approx 0.3\text{-}0.6 \mu_B/U$ in the magnetization [29,31] and $\Delta\rho \approx 100 \mu\Omega \text{ cm}$ in the residual resistivity [30], and by a large enhancement of the effective mass [29,30,32]. The empirical and almost universal relation $1 \text{ T} \leftrightarrow 1 \text{ K}$ between H_m and the temperature $T_{\chi}^{max} \approx 35$ K at the maximum in the magnetic susceptibility [33], also observed for a large number of heavy-fermion paramagnets [34], indicates that the CPM regime delimited by H_m and T_{χ}^{max} is, within a first approximation, controlled by a single energy scale. For $\mathbf{H} \parallel \mathbf{b}$, superconductivity is reinforced above 15 T and it abruptly disappears in the polarized paramagnetic regime above H_m [31,35]. In the following, we will label SC1 and SC2 the respective low-field and high-field regions of the superconducting phase for $\mathbf{H} \parallel \mathbf{b}$. Calorimetric studies showed the appearance under pressure of a second superconducting phase in zero magnetic field, whose critical temperature T_{sc} reaches 3 K at a pressure $p \approx 1.2$ GPa [36]. The extrapolation of the boundary between these two superconducting phases from TDO measurements under pressure and magnetic field [37] may indicate a link between the superconducting phase induced under pressure and the ambient pressure superconducting region SC2. However, to date there is no definitive experimental evidence of a transition between two different superconducting phases SC1 and SC2 at ambient pressure. Alternatively, the upturn in the critical field, which is controlled by a tight balance between the orbital limitation of H_{c2} and the increase of the pairing strength with field [35], could also be induced by a smooth increase of the strong coupling constant λ .

Figure 1(b) presents a combination of low-temperature magnetic-field versus field-angle phase diagrams of UTe_2 obtained in Refs. [31,35]. It summarizes the effect of magnetic fields applied in the (\mathbf{a},\mathbf{b}) and (\mathbf{b},\mathbf{c}) planes. A key property is that the metamagnetic field H_m has a minimal value for $\mathbf{H} \parallel \mathbf{b}$. It strongly increases when the field is tilted from \mathbf{b} towards the easy magnetic axis \mathbf{a} , and exceeds the maximum measured field (60 T) for $\phi = (\mathbf{b},\mathbf{a}) > 20^\circ$. The increase of H_m is softer when the field is tilted from \mathbf{b} towards \mathbf{c} , where it can be followed up to angles $\theta = (\mathbf{b},\mathbf{c}) \approx 50^\circ$. At small angles ϕ and θ , the field-reinforcement of superconductivity rapidly disappears, and the superconducting critical field shows an almost step-like decrease from 35 T to $\simeq 15$ T. For larger angles H_{c2} decreases smoothly reaching values of 6 and 10 T for $\mathbf{H} \parallel \mathbf{a}$ and $\mathbf{H} \parallel \mathbf{c}$, respectively. A similar suppression of the field-reinforced superconducting phase was reported by tilting the magnetic field away from \mathbf{b} in UCoGe [11]. For the three field-directions \mathbf{a} , \mathbf{b} , and \mathbf{c} , the low-temperature critical fields $\mu_0 H_{c2,a} \approx 6$ T, $\mu_0 H_{c2,c} \approx 10$ T, and $\mu_0 H_{c2,b} \approx 15\text{-}20$ T (i.e., the extrapolated value of $\mu_0 H_{c2,b}$ ignoring the field-reinforcement below 300 mK) delimiting the low-field superconducting phase SC1 are inversely-correlated with the low-temperature magnetic susceptibilities $\chi_a > \chi_c > \chi_b$ (see Figure 1 and [23,29,33]). A similar inverse relation between the magnetic anisotropy and the anisotropy of H_{c2} was observed in other heavy-fermion superconductors, as URu_2Si_2 [38,39], CeCoIn_5 [40,41], UCoGe and URhGe [11,42]. Spectacularly, a second field-induced superconducting phase was reported in UTe_2 for a field direction tilted from \mathbf{b} towards \mathbf{c} by an angle θ ranging from 20° to 40° [31]. This phase, labelled here as SC-PPM, was observed only in the PPM regime, in fields higher than $\mu_0 H_m \simeq 40\text{-}45$ T, and up to a critical field of $\simeq 60$ T [31].

In the present work, we focus on a systematic study of the superconducting phases induced in UTe_2 at ambient pressure, under a magnetic field applied either along \mathbf{b} , or tilted by an angle $\theta \simeq 27 \pm 5^\circ$ from \mathbf{b} towards \mathbf{c} . We benefited from a unique combination of extreme conditions offered at the

LNCMI-Toulouse, allowing high-magnetic-field electrical resistivity measurements under almost isothermal conditions: long-duration (rise = 70 ms, fall = 300 ms) pulsed magnetic fields up to 60 T, combined with temperatures down to 200 mK. Our results in UTe₂ unambiguously show zero-resistance in the SC-PPM phase, confirming its superconducting nature. We extracted the full magnetic-field-temperature phase diagrams of UTe₂ for $\mathbf{H} \parallel \mathbf{b}$ and \mathbf{H} tilted by $\theta \simeq 27^\circ$ from \mathbf{b} to \mathbf{c} . From a Fermi-liquid analysis of the resistivity we determine the field dependence of the residual resistivity ρ_0 and estimate the variation of the effective mass m^* [43]. These quantities show striking similarities for the two field-directions in contrast with the very different superconducting phase diagrams. In the discussion, we give some elements for the theoretical challenge to understand the nature of these two field-induced superconducting phases in UTe₂.

Results

Low-temperature and high-magnetic-field electrical resistivity

The magnetic-field variation of the electrical resistivity ρ of UTe₂ single crystals, measured with a current injected along the \mathbf{a} -direction, is presented in Figure 2. Data obtained for the two magnetic field directions, $\mathbf{H} \parallel \mathbf{b}$ and \mathbf{H} tilted by $\theta = 27 \pm 5^\circ$ from \mathbf{b} in the (\mathbf{b}, \mathbf{c}) plane are shown in Figure 2(a-b) and Figure 2(c-d), respectively, for a large range of temperatures varying from 200 mK to 80 K. A comparison of field-up and field-down data (see Supplemental Information) shows almost no heating of the samples by eddy currents in our low-temperature data, which were obtained in long-duration pulsed magnetic fields. At temperatures from $T = 2.2$ K to $T_{CEP} \approx 5$ -6 K, at which a critical end-point is observed in the present set of data, and under magnetic fields $\mathbf{H} \parallel \mathbf{b}$ and \mathbf{H} tilted by $\theta = 27 \pm 5^\circ$, similar and sharp first-order step-like increases of ρ are observed at the metamagnetic field $\mu_0 H_m$, which equals 34 and 45 T for the two field directions, respectively. For both directions, when the temperature is increased above T_{CEP} , the sharp anomaly at H_m is transformed into a broad maximum, at a field also labeled H_m , which vanishes at temperatures higher than 30 K. Below we focus on the signatures of superconductivity in the low-temperature data.

Figure 2(b) shows that, for $\mathbf{H} \parallel \mathbf{b}$, field-induced superconductivity develops just below H_m , with an onset at a maximal temperature of 1.2 K and a zero-resistivity reached below the maximal superconducting temperature $T_{SC} \simeq 1$ K. In spite of a non-zero resistivity due to small out-of-phase contamination of the signal, this new set of data confirms, in magnetic fields extended up to 60 T, the two recent reports of field-reinforcement of superconductivity in UTe₂ for $\mathbf{H} \parallel \mathbf{b}$ [31,35]. For \mathbf{H} tilted by $\theta = 27 \pm 5^\circ$ from \mathbf{b} in the (\mathbf{b}, \mathbf{c}) plane, Figure 2(d) shows unambiguously a zero-resistivity regime in fields higher than H_m , whereas zero resistance was not obtained in the pioneering work [31], possibly due to heating and/or out-of-phase contamination of the signal. These data support the presence of a field-induced superconducting phase SC-PPM above H_m [31]. After an onset at a maximal temperature of 2 K, zero-resistivity is reached below the maximal superconducting temperature $T_{SC} \simeq 1.5$ K, which is higher than the superconducting temperature reported at any field applied along \mathbf{b} . The magnetic field at which the zero-resistivity superconducting phase SC-PPM develops is locked to the value $\mu_0 H_m \simeq 45$ T observed for $T > T_{SC}$. Inside the CPM regime, the onset of the phase SC-PPM at $\simeq 43$ T precedes the zero-resistivity-state reached beyond H_m . We also confirm that the low-field superconducting phase SC1 is well-separated from the field-induced phase SC-PPM. At the lowest temperature, the phase SC1 vanishes at a moderate critical field of $\simeq 10$ T.

Temperature-magnetic field phase diagrams and quantum critical fluctuations

Figure 3(a) presents the magnetic-field-temperature phase diagram extracted here for UTe₂ in a field $\mathbf{H} \parallel \mathbf{b}$. The phase diagram shows two domes corresponding to the superconducting regions SC1 at low-field and SC2 induced by a magnetic field. The transition temperature T_{SC} of SC2 is maximal at a magnetic field just below $\mu_0 H_m = 34$ T. SC2 is presumably driven by the magnetic fluctuations induced on approaching the metamagnetic transition, which also control the enhancement of the Sommerfeld coefficient γ in the heat capacity [34] and of the coefficient A of the Fermi liquid T^2 term of the electrical resistivity [30]. We confirm here that SC2 is strictly bounded by H_m , at which the magnetization was found to jump from 0.4 to 1 μ_B/U and above which a PPM regime is reached [29].

Figure 3(b) presents the magnetic field - temperature phase diagram extracted here for UTe₂ in a field \mathbf{H} tilted by $\theta = 27 \pm 5^\circ$ from \mathbf{b} in the (\mathbf{b}, \mathbf{c}) plane. While the low-field superconducting phase SC1 vanishes at a critical field $H_{c2} \simeq 10$ T, $\mu_0 H_m$ reaches 45 T at low temperature for this field direction. When the temperature is increased, the behavior is similar to that reported for $\mathbf{H} \parallel \mathbf{b}$: H_m loses its first-order character at the temperature $T_{CEP} \approx 5-6$ K. It transforms into a cross-over at higher temperatures and finally disappears above 20-30 K. In agreement with the previously-published data [31], the superconducting phase SC-PPM is only observed in fields higher than H_m , and up to a superconducting critical field higher than 60 T at low temperature. A maximal field-induced superconducting temperature $T_{SC} \approx 1.5$ K appears at a field close to H_m , emphasizing a direct link with the metamagnetic transition.

In many heavy-fermion magnets, a maximum of the effective mass is observed in the vicinity of a magnetic instability. It is commonly understood as resulting from the quantum critical magnetic fluctuations, coupled or not with a Fermi surface instability [44]. Within a Fermi-liquid description, the electrical resistivity can be fitted by $\rho(T) = \rho_0 + AT^2$, and the A coefficient varies as the square of the effective mass m^* . In heavy-fermion systems, m^* is mainly controlled by magnetic fluctuations related with the proximity of quantum magnetic instabilities. We note that considering the coefficient A can lead to an overestimation of m^* [45]. Figures 3(a) and 3(b) present the magnetic-field variations of A and ρ_0 , respectively, extracted here for UTe₂ with $\mathbf{H} \parallel \mathbf{b}$ and \mathbf{H} tilted by $\theta = 27 \pm 5^\circ$ from \mathbf{b} to \mathbf{c} . Fermi-liquid-like fits to the high-field resistivity data were done for all fields investigated here, in the temperature windows $1.5 \leq T \leq 4.2$ K for $\mathbf{H} \parallel \mathbf{b}$, and $2.2 \leq T \leq 4.2$ K for \mathbf{H} tilted by $\theta = 27^\circ$ (see Supplemental Material). We find almost similar field-variations of A and ρ_0 for the two field directions: at H_m , while A increases by a factor $\simeq 6$ and passes through a sharp maximum, ρ_0 undergoes a sharp step-like enhancement, jumping from 15 to 80 $\mu\Omega \cdot \text{cm}$. The field-variation of A reported here for $\mathbf{H} \parallel \mathbf{b}$ is in good agreement with a previous report [30], and it indicates a sharp and strong enhancement of the magnetic fluctuations at H_m . For $\mathbf{H} \parallel \mathbf{b}$, a qualitatively similar enhancement of m^* at H_m was found by applying a Maxwell relation to magnetization data [29] and by direct heat-capacity measurements [32].

Differences between the two field-directions are visible from plots of A and ρ_0 versus H/H_m [Figures 4(a) and 4(b)]. While the variation of A through H_m is almost symmetric for $\mathbf{H} \parallel \mathbf{b}$, it is slightly asymmetric for \mathbf{H} tilted by $\theta = 27 \pm 5^\circ$ from \mathbf{b} . For the tilted-field direction, $A(H)$ is steeper for $H < H_m$ and more gradual for $H > H_m$. As well, the decrease of ρ_0 beyond H_m is more marked for \mathbf{H} tilted

by $\theta = 27 \pm 5^\circ$ from **b**. New high-field experiments are now needed for a complete angular study of the Fermi-liquid behavior.

Discussion

The ultimate goal would be to provide a full microscopic description of the different superconducting phases and their pairing mechanisms in UTe₂. We are still far from this objective, but the experimental data presented here, in complement to those from [31], offer a broad set of constraints for theories. A striking feature of the phase diagrams presented in Figures 3(a-b) is that the superconducting phases SC2 for **H** || **b** and SC-PPM in a field **H** tilted by $\theta = 27 \pm 5^\circ$ from **b** towards **c** are bounded by the metamagnetic field H_m , with a substantial difference that the phase SC2 is pinned inside the CPM regime and it does not survive in the PPM regime while, inversely, the phase SC-PPM is pinned inside the PPM regime and does not develop in the CPM regime. A natural explanation would be that the pairing mechanism changes drastically on crossing the first-order line H_m , at which one would expect a difference in the nature of the critical magnetic fluctuations in the CPM and PPM regimes. This difference would change substantially for the two field-directions **H** || **b** and **H** tilted by 27° from **b**.

A rough estimation of the field-dependence of the pairing strength can be obtained from the Fermi-liquid analysis done above, where a maximum of the quadratic coefficient A at the metamagnetic transition indicated an increase of the effective mass m^* , presumably controlled by critical magnetic fluctuations. In a simple picture, the effective mass can be related by $m^* \sim 1 + \lambda$ to the superconducting pairing strength λ [46,47]. However, the fact that the enhancement of A is almost symmetric around H_m is puzzling with respect to the abrupt suppression of superconductivity for **H** || **b**, and its abrupt appearance for **H** tilted by $\theta = 27 \pm 5^\circ$ from **b** towards **c**. A similar symmetrical enhancement of A has been observed at the metamagnetic transition in other heavy fermion systems, where a drastic change of magnetic fluctuations and Fermi surfaces was found [48,49]. The abrupt disappearance/appearance of superconductivity at H_m could also result from a sudden change of the Fermi surface. A Fermi surface reconstruction is compatible with the large and sudden variation of the residual resistivity at H_m for the two field directions, but also with the sign changes in the thermoelectric power and Hall coefficient at H_m for **H** || **b** [50]. However our results raise a serious hurdle to both these pictures since the field-driven enhancement of A is very similar for **H** || **b** and **H** tilted by $\theta = 27 \pm 5^\circ$ from **b** to **c**. The asymmetry in the field-variation of A for **H** tilted by 27° suggests that the magnetic fluctuations may be slightly more intense above H_m for this field direction, but this effect is too small to explain the differences between the phases SC2 and SC-PPM. The magnetization jump at H_m is also very similar for **H** || **b** and **H** tilted by 27° [31]. Extra ingredients are, thus, needed to describe the field and angle domains of stability of these two field-induced superconducting phases. In the following, we mention elements that may be considered for such description.

Figure 5 presents views of the crystal structure of UTe₂ where the magnetic uranium ions can be seen to form a ladder structure [51]. We highlight the family of reticular (and cleaving) planes of Miller indices (0 1 1), which contain sets of ladders having the smallest inter-ladder U-U distance ($d_3 = 4.89 \text{ \AA}$). Interestingly, the direction **n** normal to these planes coincides, within the experimental uncertainty, with the field-direction along which the phase SC-PPM develops [31]. It lies in the (**b,c**) plane and has an angle $\theta = 23.7^\circ$ with **b** (see Supplementary Information). Although the connection with the pairing mechanism remains unclear, this coincidence may not be accidental and may constitute a possible line of approach for future theories.

In relation with the ladder structure, magnetic frustration has been invoked as a possible origin of the paramagnetic ground state in UTe_2 at zero field and ambient pressure, and a competition between ferromagnetic and antiferromagnetic configurations has been discussed [51,52]. Electronic structure calculations pointed out that the ground state is sensitive to the Coulomb repulsion, and that the ferromagnetic and antiferromagnetic configurations are energetically-close [51]. The respective roles of ferromagnetic and antiferromagnetic fluctuations in UTe_2 may, thus, be important for the superconducting phases, and this question needs to be clarified. While UTe_2 was first proposed to be nearly-ferromagnetic [23], the nature of the pressure-induced magnetic phase, initially reported in [36], was not determined so far. Several studies suggested that UTe_2 is not a simple ferromagnet and may be close to an antiferromagnetic instability [53,54,55]. At ambient pressure, the absence of metamagnetism in a magnetic field up to 55 T applied along the easy magnetic axis \mathbf{a} [29,30] indicates that UTe_2 is at least not a conventional Ising paramagnet close to a ferromagnetic instability, unlike UGe_2 under pressure [56] and $UCoAl$ at ambient pressure [57]. The negative Curie-Weiss temperatures extracted from the high-temperature magnetic susceptibility, for the three directions $\mathbf{H} \parallel \mathbf{a}$, \mathbf{b} , and \mathbf{c} [see Figure 1(a)], indicate antiferromagnetic exchange interactions (see also [33,58]). A broad maximum at the temperature $T_\chi^{max} = 35$ K in the magnetic susceptibility for $\mathbf{H} \parallel \mathbf{b}$ is also compatible with the onset of antiferromagnetic fluctuations, as observed in several heavy-fermion paramagnets [34]. Low-temperature downward deviations of the magnetic susceptibility for $\mathbf{H} \parallel \mathbf{a}, \mathbf{c}$ (in comparison with its high-temperature behavior) are observed in the log-log plot shown in Inset of Figure 1(a). These deviations confirm the formation of a heavy-fermion state below 50 K, which may coincide with the onset of antiferromagnetic fluctuations. Interestingly, the high-temperature magnetic susceptibility for $\mathbf{H} \parallel \mathbf{a}$ varies as $1/T^{0.75}$ over more than one decade, from 20 to 300 K. However, further investigations would be needed to understanding this power-law behavior.

The different superconducting regimes may correspond to different order parameters, with different sensitivities to a magnetic field. It has been generally assumed that all the superconducting phases in UTe_2 have a triplet order parameter, mainly because of high values of the superconducting upper critical field, a small decrease of the NMR Knight shift below T_{SC} [27] and a supposed proximity to ferromagnetism [23,24,51,59]. However, this still needs confirmation especially if, as pointed out above, antiferromagnetic fluctuations may play a much larger role than initially thought. The disappearance of superconducting phase SC2 as the PPM regime is entered for $\mathbf{H} \parallel \mathbf{b}$ could indicate that some paramagnetic limiting effect is present. Thereafter, for \mathbf{H} tilted by $\theta = 27 \pm 5^\circ$ from \mathbf{b} to \mathbf{c} the phase SC-PPM could be a natural candidate for triplet superconductivity with no paramagnetic limitation. However, two questions remain: why this phase appears only for such a specific angular range, possibly in relation with the previous symmetry considerations, and especially why this phase does not develop in fields smaller than H_m ?

A full understanding of the magnetic fluctuations and their feedback on the superconducting pairing undoubtedly requires the knowledge of the Fermi surface and electronic structure of UTe_2 . As mentioned above, calculated Fermi surfaces strongly depend on the Coulomb repulsion U [51,52,60]. Two-dimensional Fermi surfaces along \mathbf{c} , similar to that of $ThTe_2$ and corresponding to a localized f -electrons limit, are expected for large values of U [51,52,61]. For quasi one-dimensional [62] or quasi two-dimensional [63] Fermi surfaces, it is predicted that the orbital limit could be suppressed for particular field directions, which may help explaining both superconducting regions SC2 and SC-PPM. However, the validity of such models was not proven so far, and no evidence for low-dimensional features in UTe_2 was found from bulk properties. An alternative scenario to describe the absence of paramagnetic limitation could be based on the combination of a Jaccarino-Peter

compensation with a field dependent pairing strength in the polarized phase. Such analysis was recently proposed to reproduce the critical superconducting fields of UTe_2 in the (\mathbf{b}, \mathbf{c}) plane [64].

Although the measurements presented here and in other works start to bring a clear picture of the complex phase diagram of UTe_2 , which includes multiple superconducting and magnetic phases, we are still far from a deep understanding of its electronic properties. A target is now to perform microscopic studies to identify the nature of the magnetic fluctuations, their change through H_m , and the superconducting order parameters. Theoretical developments are also needed to determine the superconducting pairing mechanism(s). This is a stiff challenge but the rare flurry of stunning phenomena observed in UTe_2 fully justifies such forthcoming efforts.

Methods

Samples. Single crystals of UTe_2 were prepared by the chemical vapor transport method with similar parameters as described in Ref. [23]. Their structure and orientation was checked by single-crystal X-ray diffraction. A sharp bulk transition at $T_{sc} = 1.6$ K was indicated from specific heat measurements, while zero-resistivity at temperatures below T_{sc} was confirmed by zero-field AC resistivity measurements.

Pulsed-field experiments. Magnetoresistance measurements were performed at the Laboratoire National des Champs Magnétiques Intenses (LNCMI) in Toulouse under long-duration pulsed magnetic fields, either up to 68 T (30 ms rise and 100 ms fall) and combined with an ^4He cryostat offering temperatures down to 1.4 K, or up to 58 T (55 ms rise and 300 ms fall) and combined by a home-developed dilution fridge made of a non-metallic mixing chamber offering temperatures down to 100 mK. A standard four-probe method with currents $\mathbf{I} \parallel \mathbf{a}$, at a frequency of 20–70 kHz, and a digital lock-in detection were used. Resistivity data were normalized so that the maximal value, at a temperature of ≈ 65 K and at zero-field, reaches $450 \mu\Omega\cdot\text{cm}$ (a different normalization lead to a maximum of $650 \mu\Omega\cdot\text{cm}$ in a previous work [30]). Normalization was made following absolute resistivity measurements on samples whose geometrical shape was known.

Data availability. Data and materials concerning the experiments can be available by directly contacting W. Knafo (william.knafo@lncmi.cnrs.fr.).

Acknowledgments

We acknowledge A. Miyake, J. Béard, F. Hardy, J.-P. Brison, K. Ishida, Y. Tokunaga, Y. Yanase, and H. Harima for useful discussions.

This work at the LNCMI was supported by the “Programme Investissements d’Avenir” under the project ANR-11-IDEX-0002- 02 (reference ANR-10-LABX-0037-NEXT). We acknowledge the financial support of the Cross-Disciplinary Program on Instrumentation and Detection of CEA, the French Alternative Energies and Atomic Energy Commission, and KAKENHI (JP15H05882, JP15H05884, JP15K21732, JP16H04006, JP15H05745, JP19H00646).

Author contributions

Samples were grown by G.L in close collaboration with D.A. They were characterized in zero and low fields by G.L., M.V., D.B. and G.K. Samples measured in pulsed fields were prepared by M.V.

Experiments in pulsed magnetic field were performed by W.K., M.N., and A.Z.. Data were analyzed by W.K. The paper was written by W.K. and D.B., with contributions from all of the authors.

Competing financial interests: There are no competing financial interests.

References

1. Stewart, G.R. Unconventional superconductivity, *Advances in Physics*, **66**, 75-196, (2017).
2. Flouquet, J., On the heavy-fermion road. *Prog. Low Temp. Phys.* **15**, 139-281 (2005).
3. Pfleiderer, C., Superconducting phases of f-electron compounds. *Rev. Mod. Phys.* **81**, 1551 (2009).
4. Keimer, B., Kivelson, S.A., Norman, M.R., Uchida, S., & Zaanen, From quantum matter to high-temperature superconductivity in copper oxides. *J. Nature* **518**, 179 (2015).
5. Johnston, D.C., The puzzle of high temperature superconductivity in layered iron pnictides and chalcogenides. *Adv. Phys.* **59**, 803 (2010).
6. Li, D., Lee, K., Wang, B. Y., Osada, M., Crossley, S., Lee, H. R., Cui, Y., Hikita, Y. & Hwang, H. Y. Superconductivity in an infinite-layer nickelate. *Nature* **572**, 624 (2019).
7. Cao, Y., Fatemi, V., Fang, S., Watanabe, K., Taniguchi, T., Kaxiras, E. & Jarillo-Herrero, P. Unconventional superconductivity in magic-angle graphene superlattices. *Nature* **556**, 43 (2018).
8. Saxena, S., Agarwal, P., Ahilan, K., Grosche, F., Haselwimmer, R., Steiner, M., Pugh, E., Walker, I., Julian, S., Monthoux, P., Lonzarich, G., Huxley, A., Sheikin, I., Braithwaite, D., & Flouquet, J. Superconductivity on the border of itinerant-electron ferromagnetism in UGe₂. *Nature* **406**, 587 (2000).
9. Aoki, D., Huxley, A., Ressouche, E., Braithwaite, D., Flouquet, J., Brison, J.P., Lhotel, E., & Paulsen, C. Coexistence of superconductivity and ferromagnetism in URhGe. *Nature* **413**, 613 (2001).
10. Huy, N.T., Gasparini, A., de Nijs, D.E., Huang, Y., Klaasse, J.C.P., Gortemulder, T., de Visser, A., Hamann, A., Görlach, T., & v. Löhneysen, H. Superconductivity on the Border of Weak Itinerant Ferromagnetism in UCoGe. *Phys. Rev. Lett.* **99**, 067006 (2007).
11. Aoki, D., Ishida, K., & Flouquet, J. Review of U-based Ferromagnetic Superconductors: Comparison between UGe₂, URhGe, and UCoGe. *J. Phys. Soc. Jpn.* **88**, 022001 (2019).
12. Sheikin, I., Huxley, A., Braithwaite, D., Brison, J.P., Watanabe, S., Miyake, K., & Flouquet, J. Anisotropy and pressure dependence of the upper critical field of the ferromagnetic superconductor UGe₂. *Phys. Rev. B* **64**, 220503(R) (2001).
13. Lévy, F., Sheikin, I., Grenier, B., & Huxley, A.D. Magnetic Field-Induced Superconductivity in the Ferromagnet URhGe. *Science* **309**, 1343 (2005).

14. Aoki, D., Matsuda, T.D., Taufour, V., Hassinger, E., Knebel, G. & Flouquet, J. Extremely Large and Anisotropic Upper Critical Field and the Ferromagnetic Instability in UCoGe. *J. Phys. Soc. Jpn.* **78**, 113709 (2009).
15. Miyake, A., Aoki, D., & Flouquet, J. Field Re-entrant Superconductivity Induced by the Enhancement of Effective Mass in URhGe. *J. Phys. Soc. Jpn.* **77**, 094709 (2008).
16. Tokunaga, Y., Aoki, D., Mayaffre, H., Krämer, S., Julien, M.-H., Berthier, C., Horvatic, M., Sakai, H., Kambe, S., & Araki, S. Reentrant Superconductivity Driven by Quantum Tricritical Fluctuations in URhGe: Evidence from ^{59}Co NMR in URh_{0.9}Co_{0.1}Ge. *Phys. Rev. Lett.* **114**, 216401 (2015).
17. Yelland, E.A., Barraclough, J.M., Wang, W., Kamenev, K.V., & Huxley, A.D. High-field superconductivity at an electronic topological transition in URhGe. *Nat. Phys.* **7**, 890 (2011).
18. Gourgout, A., Pourret, A., Knebel, G., Aoki, D., Seyfarth, G., & Flouquet, J. Collapse of Ferromagnetism and Fermi Surface Instability near Reentrant Superconductivity of URhGe. *Phys. Rev. Lett.* **117**, 046401 (2016).
19. Sherkunov, Y., Chubukov, A.V., & Betouras, J.J. Effects of Lifshitz Transitions in Ferromagnetic Superconductors: The Case of URhGe. *Phys. Rev. Lett.* **121**, 097001 (2018).
20. Knafo, W., Matsuda, T.D., Aoki, D., Hardy, F., Scheerer, G.W., Ballon, G., Nardone, M., Zitouni, A., Meingast, C., & Flouquet, J. High-field moment polarization in the ferromagnetic superconductor UCoGe. *Phys. Rev. B* **86**, 184416 (2012).
21. Hattori, T., Karube, K., Ishida, K., Deguchi, K., Sato, N.K., & Yamamura, T. Relationship between Ferromagnetic Criticality and the Enhancement of Superconductivity Induced by Transverse Magnetic Fields in UCoGe. *J. Phys. Soc. Jpn.* **83**, 073708 (2014).
22. Manago, M., Kitagawa, S., Ishida, K., Deguchi, K., Sato, N.K., & Yamamura, T. Spin-triplet superconductivity in the paramagnetic UCoGe under pressure studied by ^{59}Co NMR. *Phys. Rev. B* **100**, 035203 (2019).
23. Ran, S., Eckberg, C., Ding, Q.-P., Furukawa, Y., Metz, T., Saha, S.R., Liu, I.-L., Zic, M., Kim, H., Paglione, J., & Butch, N.P. Nearly ferromagnetic spin-triplet superconductivity. *Science* **365**, 684 (2019).
24. Aoki, D., Nakamura, A., Honda, F., Li, D., Homma, Y., Shimizu, Y., Sato, Y.J., Knebel, G., Brison, J.-P., Pourret, A., Braithwaite, D., Lapertot, G., Niu, Q., Vališka, M., Harima, H., & Flouquet, J. Unconventional Superconductivity in Heavy Fermion UTe₂. *J. Phys. Soc. Jpn.* **88**, 043702 (2019).
25. Sundar, S., Gheidi, S., Akintola, K., Côté, A.M., Dunsiger, S.R., Ran, S., Butch, N.P., Saha, S.R., Paglione, J., & Sonier, J.E. Coexistence of ferromagnetic fluctuations and superconductivity in the actinide superconductor UTe₂. *Phys. Rev. B* **100**, 140502(R) (2019).
26. Tokunaga, Y., Sakai, H., Kambe, S., Hattori, T., Higa, N., Nakamine, G., Kitagawa, S., Ishida, K., Nakamura, A., Shimizu, Y., Homma, Y., Li, D. X., Honda, F., & Aoki, D. ^{125}Te -NMR Study on a Single Crystal of Heavy Fermion Superconductor UTe₂. *J. Phys. Soc. Jpn.* **88**, 073701 (2019).

27. Nakamine, G., Kitagawa, S., Ishida, K., Tokunaga, Y., Sakai, H., Kambe, S., Nakamura, A., Shimizu, Y., Homma, Y., Li, D., Honda, F., & Aoki, D. Superconducting Properties of Heavy Fermion UTe_2 Revealed by ^{125}Te -nuclear Magnetic Resonance. *J. Phys. Soc. Jpn.* **88**, 113703 (2019).
28. Jiao, L., Howard, S., Ran, S., Wang, Z., Rodriguez, J.O., Sigrist, M., Wang, Z., Butch, N., & Madhavan, V. Chiral superconductivity in heavy-fermion metal UTe_2 . *Nature* **579**, 523 (2020).
29. Miyake, A., Shimizu, Y., Sato, Y.J., Li, D., Nakamura, A., Homma, Y., Honda, F., Flouquet, J., Tokunaga, M., & Aoki, D. Metamagnetic Transition in Heavy Fermion Superconductor UTe_2 . *J. Phys. Soc. Jpn.* **88**, 063706 (2019).
30. Knafo, W., Vališka, M., Braithwaite, D., Lapertot, G., Knebel, G., Pourret, A., Brison, J.-P., Flouquet, J., & Aoki, D. Magnetic-Field-Induced Phenomena in the Paramagnetic Superconductor UTe_2 . *J. Phys. Soc. Jpn.* **88**, 063705 (2019).
31. Ran, S., Liu, I.-L., Eo, Y.S., Campbell, D. J., Neves, P., Fuhrman, W.T., Saha, S.R., Eckberg, C., Kim, H., Paglione, J., Graf, D., Singleton, J., & Butch, N.P. Extreme magnetic field-boosted superconductivity. *Nature Physics* **15**, 1250–1254 (2019).
32. Imajo, S., Kohama, Y., Miyake, A., Dong, C., Tokunaga, M., Flouquet, J., Kindo, K., & Aoki, D. Thermodynamic Investigation of Metamagnetism in Pulsed High Magnetic Fields on Heavy Fermion Superconductor UTe_2 . *J. Phys. Soc. Jpn.* **88**, 083705 (2019).
33. Ikeda, S., Sakai, H., Aoki, D., Homma, Y., Yamamoto, E., Nakamura, A., Shiokawa, Y., Haga, Y., & Ōnuki, Y. Single Crystal Growth and Magnetic Properties of UTe_2 . *J. Phys. Soc. Jpn. [Suppl.]* **75**, 116 (2006)
34. Aoki, D., Knafo, W., & Sheikin, I. Heavy fermions in a high magnetic field. *C. R. Phys.* **14**, 53 (2013).
35. Knebel, G., Knafo, W., Pourret, A., Niu, Q., Vališka, M., Braithwaite, D., Lapertot, G., Nardone, M., Zitouni, A., Mishra, S., Sheikin, I., Seyfarth, G., Brison, J.-P., Aoki, D., & Flouquet, J. Field-Reentrant Superconductivity Close to a Metamagnetic Transition in the Heavy-Fermion Superconductor UTe_2 . *J. Phys. Soc. Jpn.* **88**, 063707 (2019).
36. Braithwaite, D., Vališka, M., Knebel, G., Lapertot, G., Brison, J.-P., Pourret, A., Zhitomirsky, M.E., Flouquet, J., Honda, F., & Aoki, D. Multiple superconducting phases in a nearly ferromagnetic system. *Communications Physics* **2**, 147 (2019).
37. Lin, W.-C., Campbell, D.J., Ran, S., Liu, I.-L., Kim, H., Nevidomskyy, A.H., Graf, D., Butch, N.P., & Paglione, J. Tuning magnetic confinement of spin-triplet superconductivity. arXiv:2002.12885.
38. Palstra, T.T., Menovsky, A.A., van den Berg, J., Dirkmaat, A.J., Kes, P.H., Nieuwenhuys, G.J., & Mydosh, J.A. Superconducting and Magnetic Transitions in the Heavy-Fermion System URu_2Si_2 . *Phys. Rev. Lett.* **55**, 2727 (1985).
39. Bastien, G. Aoki, D., Lapertot, G., Brison, J.-P., Flouquet, J., & Knebel, G. Fermi-surface selective determination of the g-factor anisotropy in URu_2Si_2 . *Phys. Rev. B* **99**, 165138 (2019).

40. Petrovic, C., Pagliuso, P.G., Hundley, M.F., Movshovich, R., Sarrao, J.L., Thompson, J.D., Fisk, Z., & Monthoux, P. Heavy-fermion superconductivity in CeCoIn₅ at 2.3 K. *J. Phys.: Condens. Matter* **13** L337–L342 (2001).
41. Howald, L., Knebel, G., Aoki, D., Lapertot, G., & Brison, J.-P. The upper critical field of CeCoIn₅. *New Journal of Physics* **13**, 113039 (2011).
42. Braithwaite, D., Aoki, D., Brison, J.-P., Flouquet, J., Knebel, G., Nakamura, A., & Pourret, A. Dimensionality Driven Enhancement of Ferromagnetic Superconductivity in URhGe. *Phys. Rev. Lett.* **120**, 037001 (2018).
43. Kadowaki, K., & Woods, S.B. Universal relationship of the resistivity and specific heat in heavy-Fermion compounds. *Solid State Commun.* **58**, 507 (1986).
44. von Löhneysen, H., Rosch, A., Vojta, M., & Wölfle, P. Fermi-liquid instabilities at magnetic quantum phase transitions. *Rev. Mod. Phys.* **79**, 1015-1075 (2007).
45. Moriya, T., & Ueda, K., Spin fluctuations and high temperature superconductivity. *Adv. Phys.* **49**, 555-606 (2000).
46. Eliashberg, G. Interactions between electrons and lattice vibrations in a superconductor. *Soviet Phys. JETP-USSR* **11**, 696–702 (1960).
47. Bulaevskii, L.N., Dolgov, O.V., & Ptitsyn, M.O. Properties of strong-coupled superconductors. *Phys. Rev. B* **38**, 11290–11295 (1988).
48. Raymond, S., Ravelson, D., Kambe, S., Regnault, L.P., Fak, B., Calemczuk, R., Flouquet, J., Haen, P., & Lejay, P. Magnetic instabilities in CeRu₂Si₂ compounds. *Physica B* **259-261**, 48 (1999).
49. Flouquet, J., Haen, P., Raymond, S., Aoki, D., & Knebel, G. Itinerant metamagnetism of CeRu₂Si₂: bringing out the dead. Comparison with the new Sr₃Ru₂O₇ case. *Physica. B Condens. Matter* **319**, 251 (2002).
50. Niu, Q., Knebel, G., Braithwaite, D., Aoki, D., Lapertot, G., Vališka, M., Seyfarth, G., Knafo, W., Helm, T., Brison, J.-P., Flouquet, J., & Pourret, A. Evidence of Fermi Surface Reconstruction at the Metamagnetic Transition of the Strongly Correlated Superconductor UTe₂. *Physical Review Research* (2020).
51. Xu, Y., Sheng, Y., & Yang, Y.-f. Quasi-Two-Dimensional Fermi Surfaces and Unitary Spin-Triplet Pairing in the Heavy Fermion Superconductor UTe₂. *Phys. Rev. Lett.* **123**, 217002 (2019).
52. Ishizuka, J., Sumita, S., Daido, A., & Yanase, Y. Insulator-Metal Transition and Topological Superconductivity in UTe₂ from a First-Principles Calculation. *Phys. Rev. Lett.* **123**, 217001 (2019).
53. Aoki, D., Honda, F., Knebel, G., Braithwaite, D., Nakamura, A., Li, D., Homma, Y., Shimizu, Y., Sato, Y.J., Brison, J.-P., & Flouquet, J. Multiple Superconducting Phases and Unusual Enhancement of the Upper Critical Field in UTe₂. *J. Phys. Soc. Jpn.* **89**, 053705 (2020).
54. Knebel, G., Kimata, M., Vališka, M., Honda, F., Li, D., Braithwaite, D., Lapertot, G., Knafo, W., Pourret, A., Sato, Y.J., Shimizu, Y., Kihara, T., Brison, J., Flouquet, J., & Aoki, D. Anisotropy of the

Upper Critical Field in the Heavy-Fermion Superconductor UTe_2 under Pressure. *J. Phys. Soc. Jpn.* **89**, 053707 (2020).

55. Thomas, S.M., Santos, F.B., Christensen, M.H., Asaba, T., Ronning, F., Thompson, J.D., Bauer, E.D., Fernandes, R.M., Fabbris, G., & Rosa, P.F.S. Evidence for a pressure-induced antiferromagnetic quantum critical point in intermediate valence UTe_2 . arXiv:2005.01659

56. Taufour, V., Aoki, D., Knebel, G., & Flouquet, J. Tricritical Point and Wing Structure in the Itinerant Ferromagnet UGe_2 . *Phys. Rev. Lett.* **105**, 217201 (2010).

57. Aoki, D., Combier, T., Taufour, V., Matsuda, T.D., Knebel, G., Kotegawa, H., & Flouquet, J., Ferromagnetic Quantum Critical Endpoint in $UCoAl$. *J. Phys. Soc. Jpn.* **80**, 094711 (2011).

58. Willa K., *et al*, to be published.

59. Metz, T., Bae, S., Ran, S., Liu, I-L., Eo, Y.S., Fuhrman, W.T., Agterberg, D.F., Anlage, S., Butch, N.P., & Paglione, J., Point-node gap structure of the spin-triplet superconductor UTe_2 . *Phys. Rev. B* **100**, 220504(R) (2019).

60. Miao, L., Liu, S., Xu, Y., Kotta, C., Kang, C.-J., Ran, S., Paglione, J., Kotliar, G., Butch, N.P., Denlinger, J.D., & Wray, L.A. Low Energy Band Structure and Symmetries of UTe_2 from Angle-Resolved Photoemission Spectroscopy. *Phys. Rev. Lett.* **124**, 076401 (2020).

61. Harima, H. How to Obtain Fermi Surfaces of UTe_2 . *JPS Conf. Proc.* **29**, 011006 (2020).

62. Lebed, A.G., & Sepper, O. Quantum limit in a magnetic field for triplet superconductivity in a quasi-one-dimensional conductor. *Phys. Rev. B*, **90**, 024510 (2014).

63. Mineev, V., to be published.

64. Brison, J.-P., *et al*, to be published.

Figures

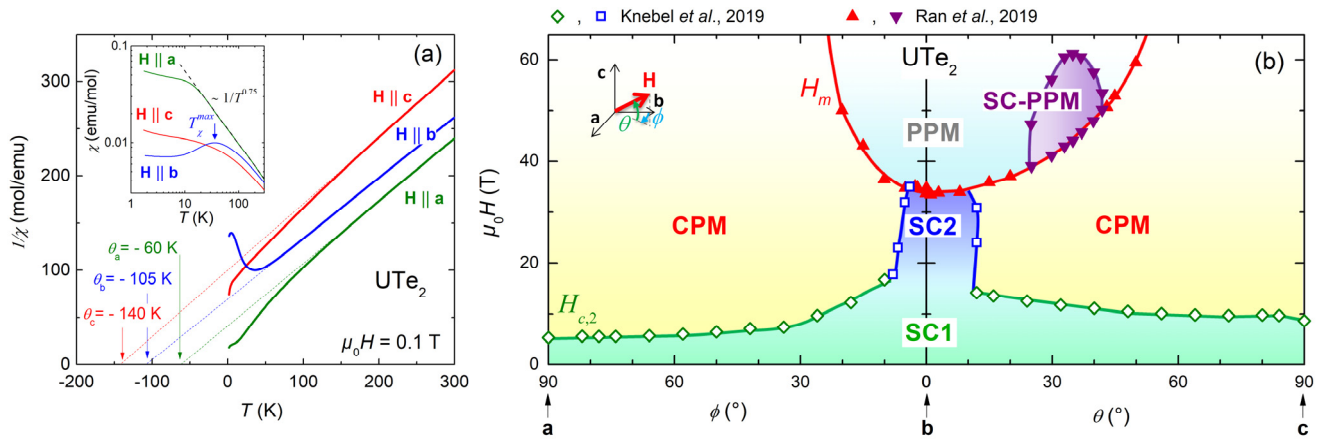


Figure 1. Magnetic susceptibility and phase diagram of UTe_2 . (a) Temperature-dependence of the inversed magnetic susceptibility $1/\chi$ of UTe_2 in magnetic fields \mathbf{H} applied along the three main crystallographic directions \mathbf{a} , \mathbf{b} , and \mathbf{c} . Inset: Temperature-dependence of the magnetic susceptibility χ for $\mathbf{H} \parallel \mathbf{a}$, \mathbf{b} , and \mathbf{c} , in a log-log scale. (b) Low-temperature magnetic phase diagram of UTe_2 , in fields applied along variable directions from \mathbf{b} to \mathbf{a} (angle ϕ) and from \mathbf{b} to \mathbf{c} (angle θ). Data from Refs. [31,34] were plotted in this Figure.

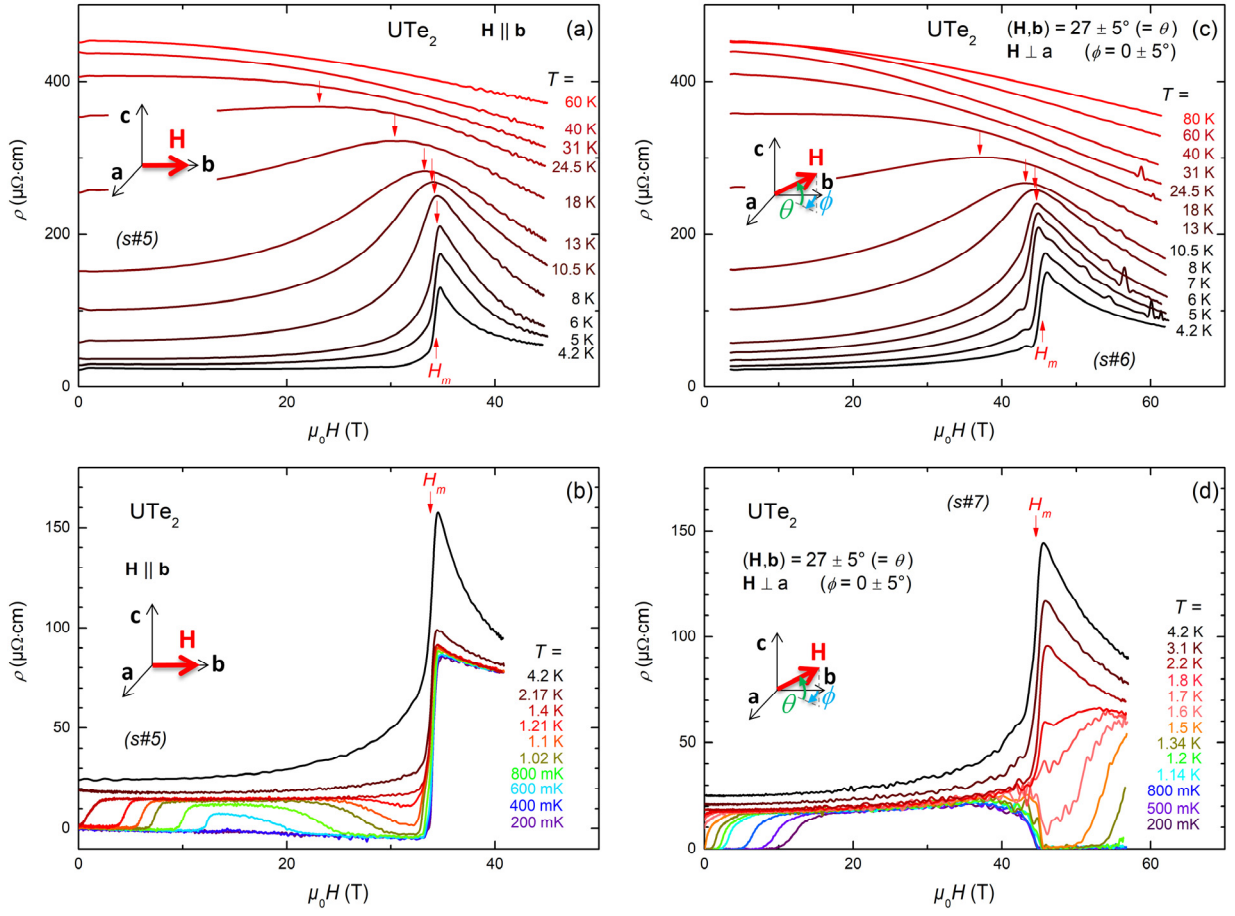


Figure 2. Electrical resistivity of UTe_2 versus magnetic field. (a) High-temperature and (b) low-temperature resistivity of UTe_2 in a magnetic field $\mathbf{H} \parallel \mathbf{b}$. (c) High-temperature and (d) low-temperature resistivity of UTe_2 in a magnetic field \mathbf{H} tilted by $27 \pm 5^\circ$ from \mathbf{b} in the (\mathbf{b}, \mathbf{c}) plane.

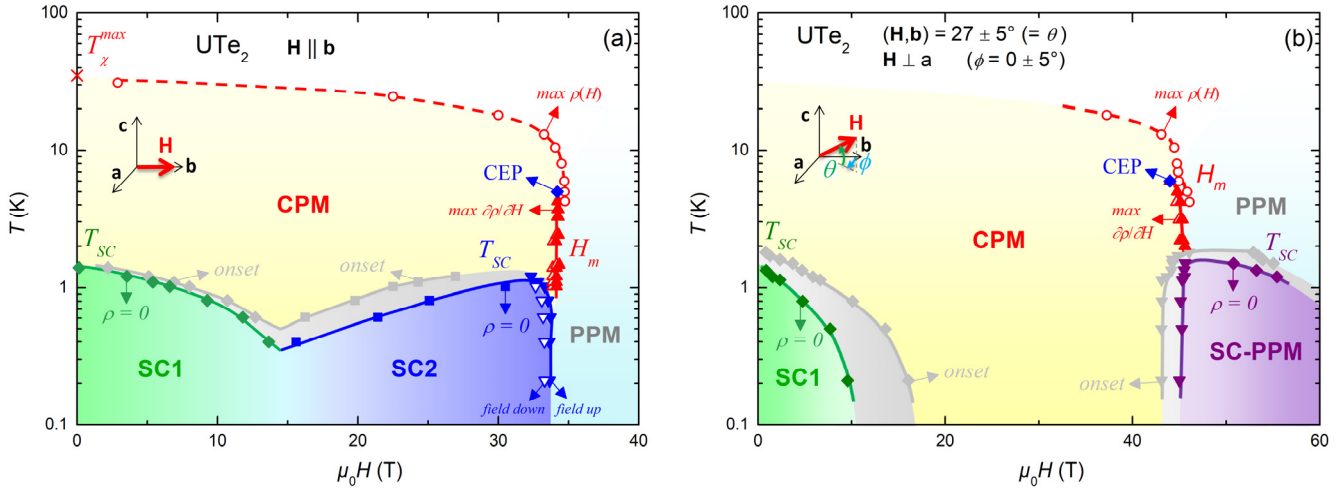


Figure 3. Magnetic phase diagrams of UTe_2 . (a) Magnetic-field-temperature phase diagram of UTe_2 in a magnetic field $\mathbf{H} \parallel \mathbf{b}$. (b) Magnetic-field-temperature phase diagram of UTe_2 in a magnetic field \mathbf{H} tilted by $27 \pm 5^\circ$ from \mathbf{b} in the (\mathbf{b}, \mathbf{c}) plane. CPM = correlated paramagnetism, PPM = polarized paramagnetism, SC1, SC2, SC-PPM indicate the different superconducting phases (or regions). CEP indicates the critical end-point of the first-order metamagnetic transition.

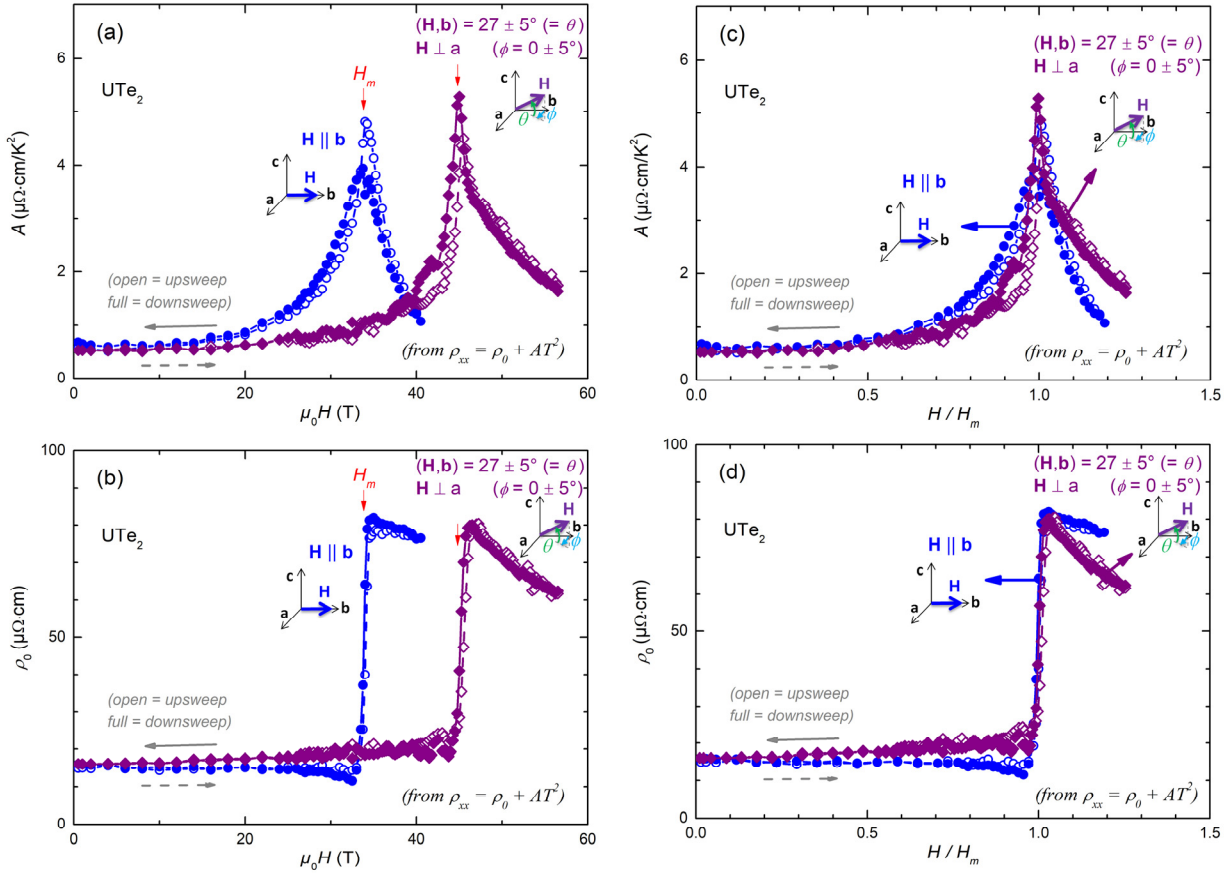


Figure 4. Quadratic coefficient A and residual resistivity of UTe_2 . (a) Magnetic-field variation of the quadratic coefficient A and (b) residual resistivity ρ_0 extracted from Fermi-liquid fits to the electrical resistivity of UTe_2 in a magnetic field $\mathbf{H} \parallel \mathbf{b}$ and in a magnetic field \mathbf{H} tilted by $27 \pm 5^\circ$ from \mathbf{b} in the (b,c) plane. Plots of (c) A and (d) ρ_0 versus H/H_m for the two field-directions. Data are presented for both field-up and field-down sweeps. Details about the Fermi-liquid fits are shown in Supplementary Figure 7 of the Supplementary Information.

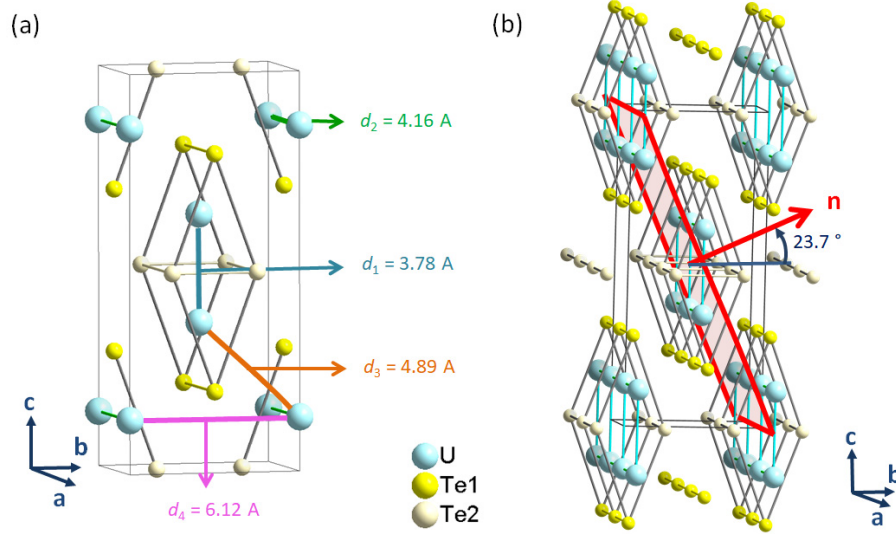


Figure 5. Crystal structure of UTe_2 . (a) Elementary unit cell and identification of 4 exchange paths corresponding to the smallest U-U distances, (b) Extended crystal structure emphasizing the network of two-leg ladders. The vector \mathbf{n} normal to a family of reticular (and cleaving) planes of Miller indices $(0\ 1\ 1)$, with an angle $\theta = (\mathbf{b}, \mathbf{n}) = 23.7^\circ$, is indicated. These reticular planes are characteristic of the ladder structure.

Supplementary Information

Comparison of two superconducting phases induced by a magnetic field in UTe_2

W. Knafo,^{1*} M. Nardone,¹ M. Valiska,² A. Zitouni,¹ G. Lapertot,² D. Aoki,^{2,3} G. Knebel,² D. Braithwaite²

¹ *Laboratoire National des Champs Magnétiques Intenses, UPR 3228, CNRS-UPS-INSA-UGA, 143 Avenue de Rangueil, 31400 Toulouse, France*

² *Univ. Grenoble Alpes and CEA, IRIG-PHELIQS, F-38000 Grenoble, France*

³ *Institute for Materials Research, Tohoku University, Ibaraki 311-1313, Japan*

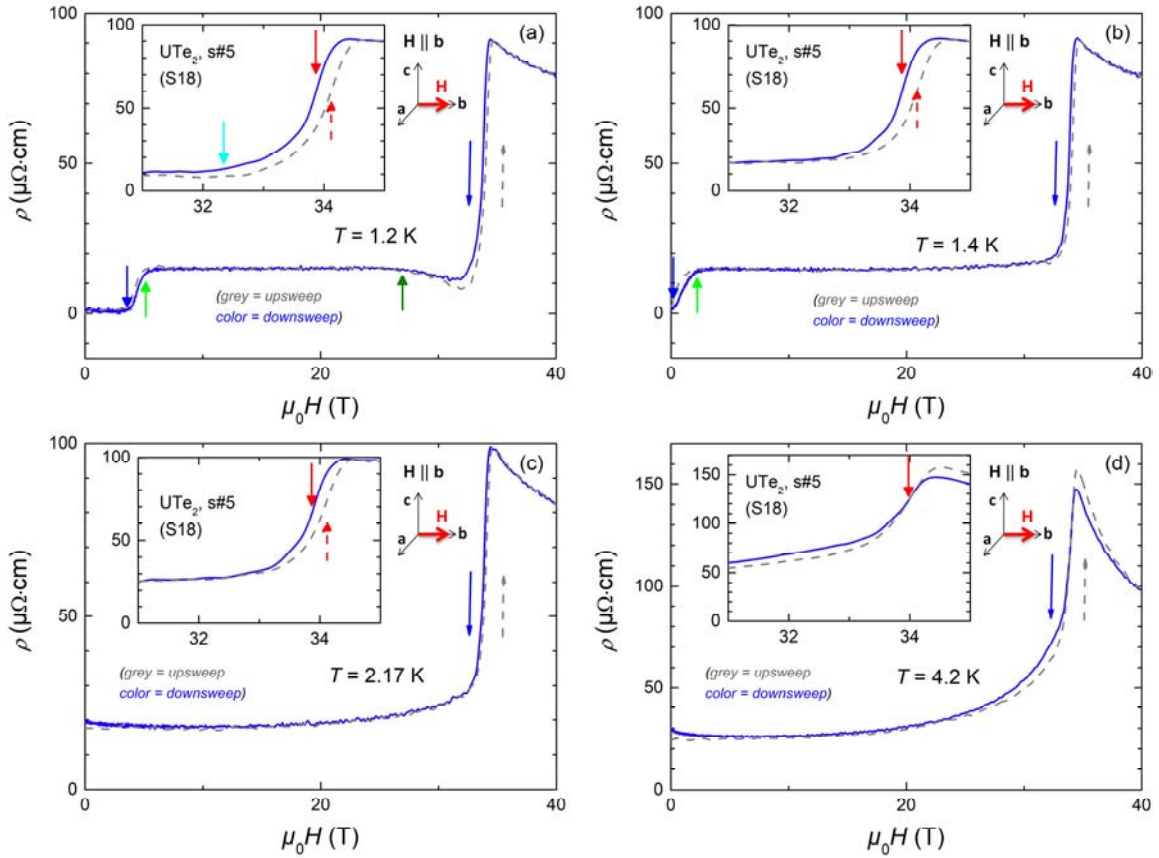
* *Corresponding author: william.knafo@lncmi.cnrs.fr*

In Supplementary Figures 1-4, we present complementary plots of the low-temperature resistivity data. In particular, a comparison of field-up and field-down data is shown, indicating almost negligible eddy current heating of the sample in the magnetic field pulses.

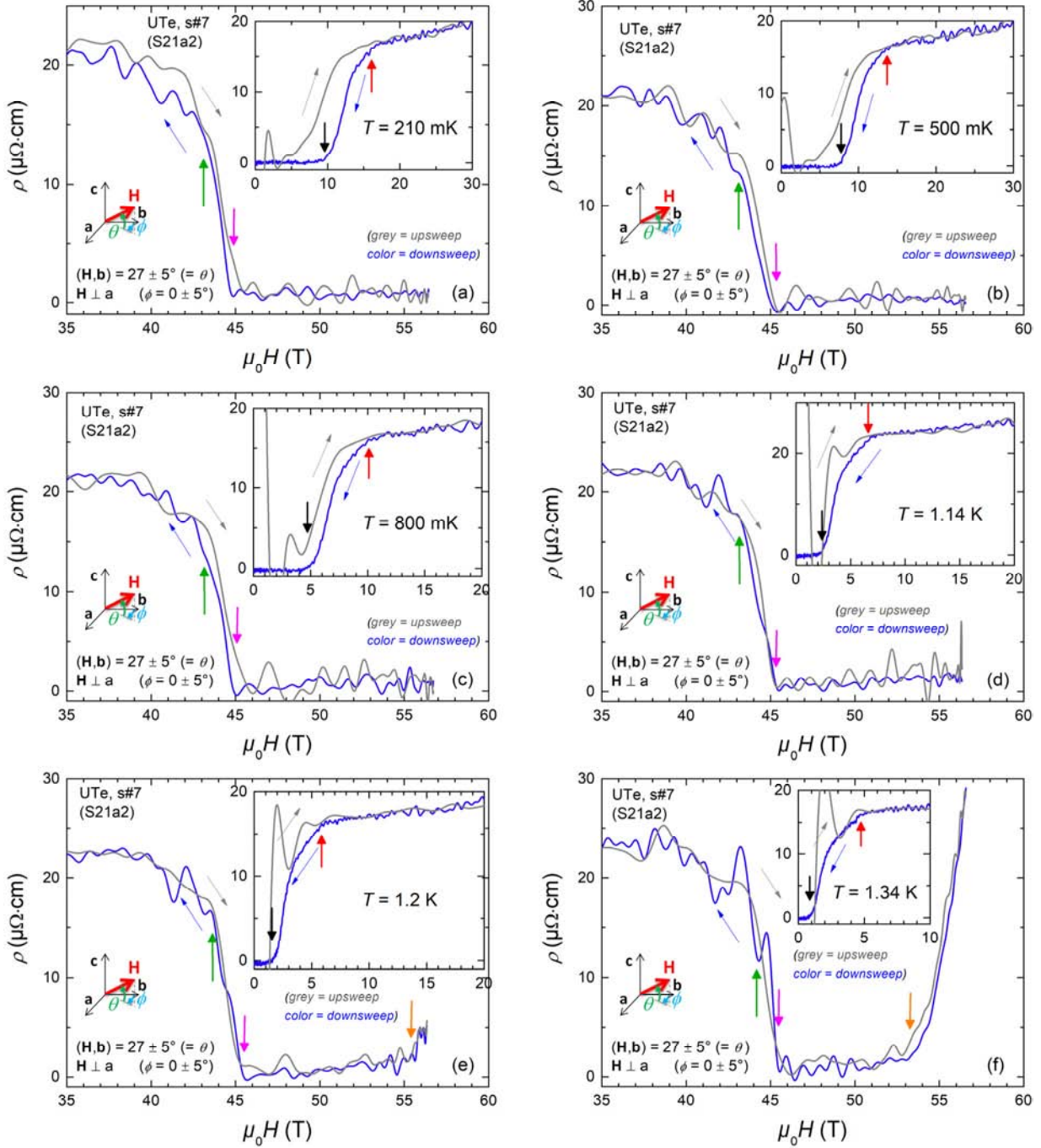
Supplementary Figure 5 (a) shows a zoom on the low-temperature resistivity of UTe_2 in a magnetic field $\mathbf{H} \parallel \mathbf{b}$ close to H_m . A small negative value of ρ is due to out-of-phase contamination in the resistive signal in high fields. At $T = 1$ and 1.4 K, a hysteresis of field width $\Delta H = 0.25$ T is visible at the first-order transition field H_m , which reaches 33.9 and 34.15 T (minimum of slope of ρ) for falling and rising fields, respectively. Supplementary Figure 5(b) shows that the hysteresis observed at H_m at $T = 1.8$ and 2.2 K is lost at low temperatures once superconductivity develops. No out-of-phase contamination is observed in this set of data.

Supplementary Figure 6 presents resistivity versus temperature plots in magnetic fields $\mathbf{H} \parallel \mathbf{b}$ and \mathbf{H} tilted by $27 \pm 5^\circ$ from \mathbf{b} in the (b,c) plane. In Supplementary Figure 7, the Fermi-liquid like fits to the electrical resistivity data are presented. These fits were used to extract the magnetic-field variations of the quadratic coefficient A and of the residual resistivity ρ_0 .

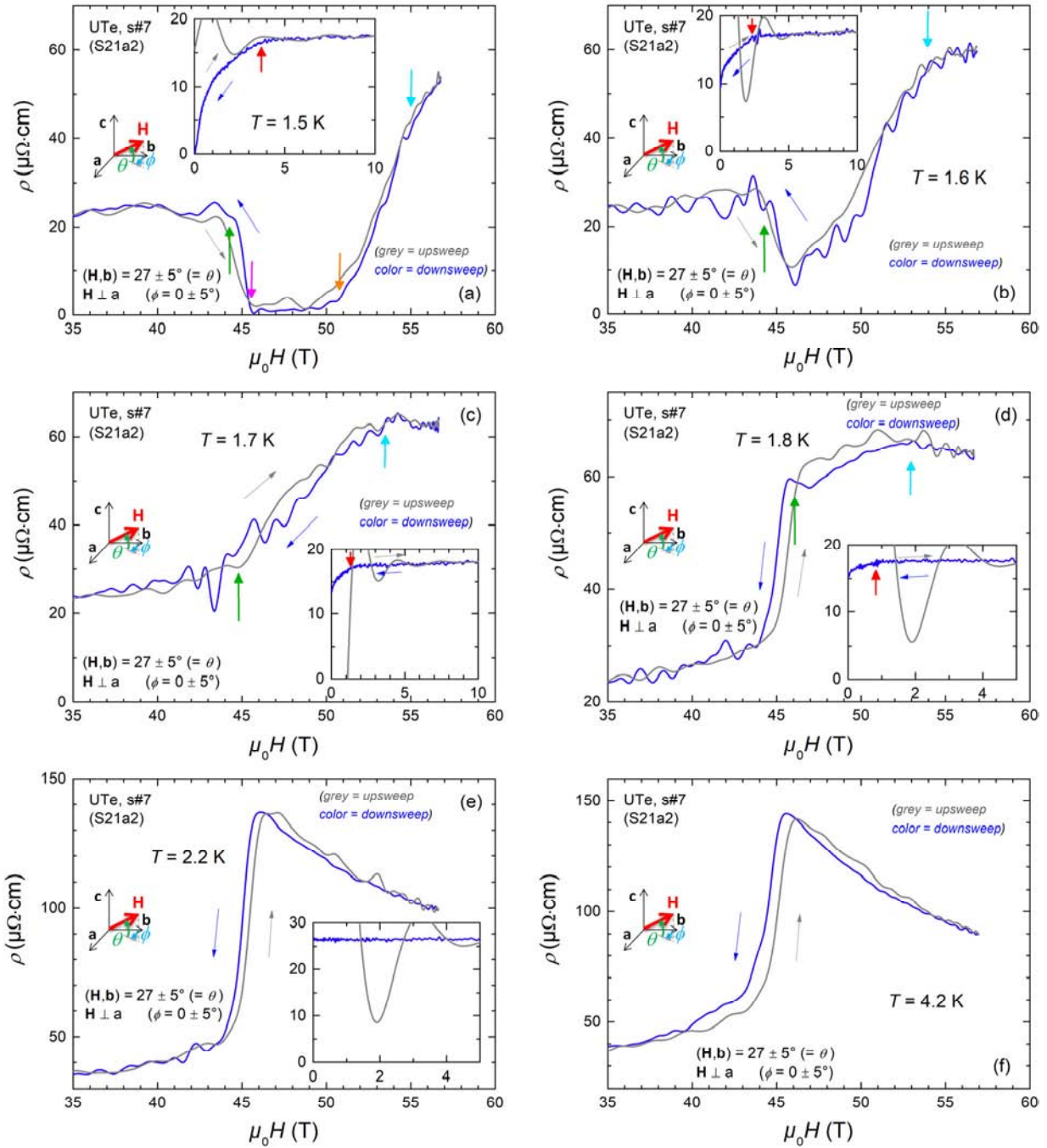
Supplementary Figure 8 presents views of the crystal structure and of the Brillouin zone, where the direction \mathbf{n} in the real space, which is equivalent to the direction $\mathbf{k} = (0 \ 1 \ 1)$ in the reciprocal space, are identified as a peculiar direction close to the direction along which a magnetic field induced the superconducting phase SC-PPM.



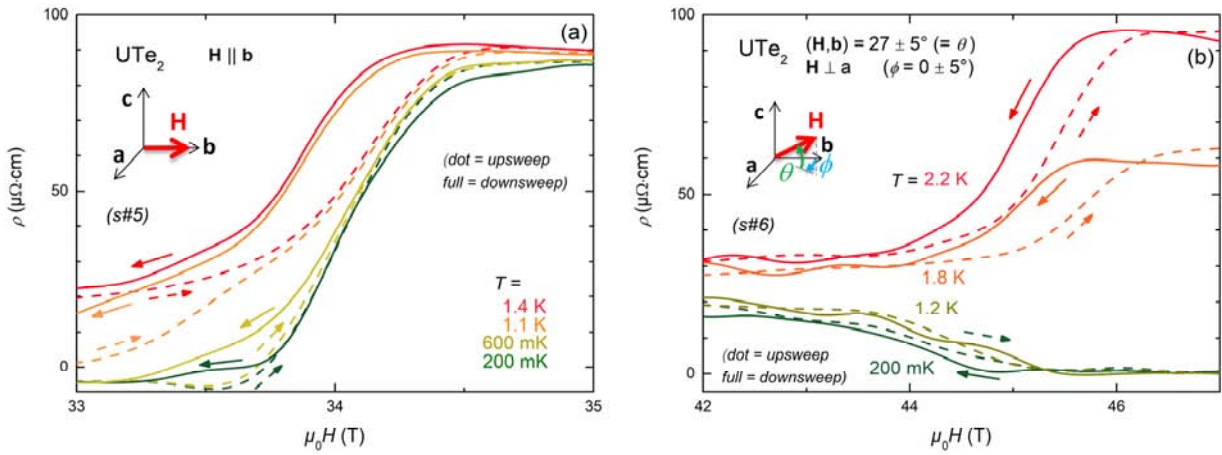
Supplementary Figure 2. Electrical resistivity of UTe_2 in a magnetic field $H \parallel b$. Comparison of field-up and field-down sweeps at temperatures from 1.2 K to 4.2 K.



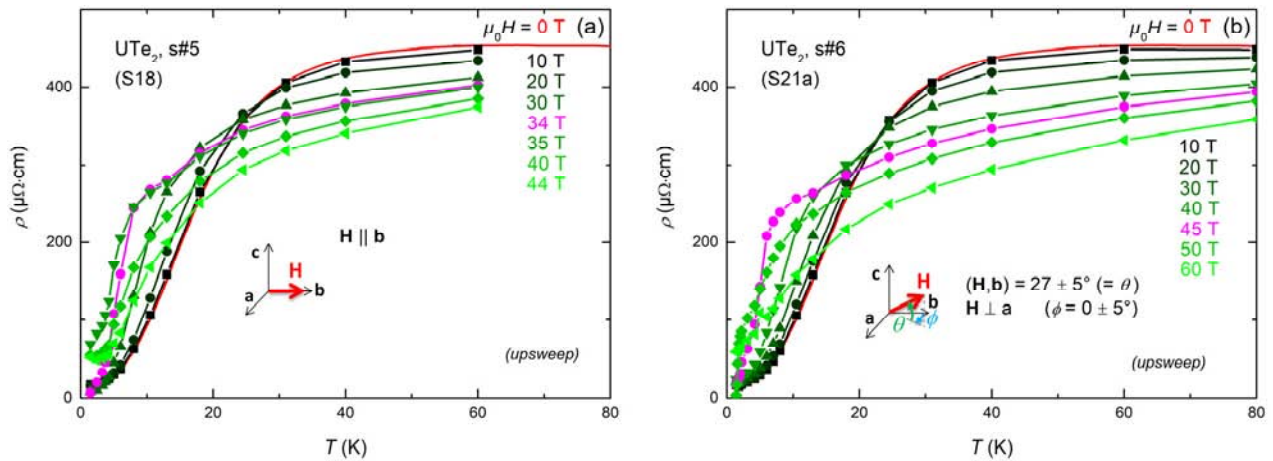
Supplementary Figure 3. Electrical resistivity of UTe₂ in a magnetic field H tilted by 27±5° from b in the (b,c) plane. Comparison of field-up and field-down sweeps at temperatures from 210 mK to 1.34 K.



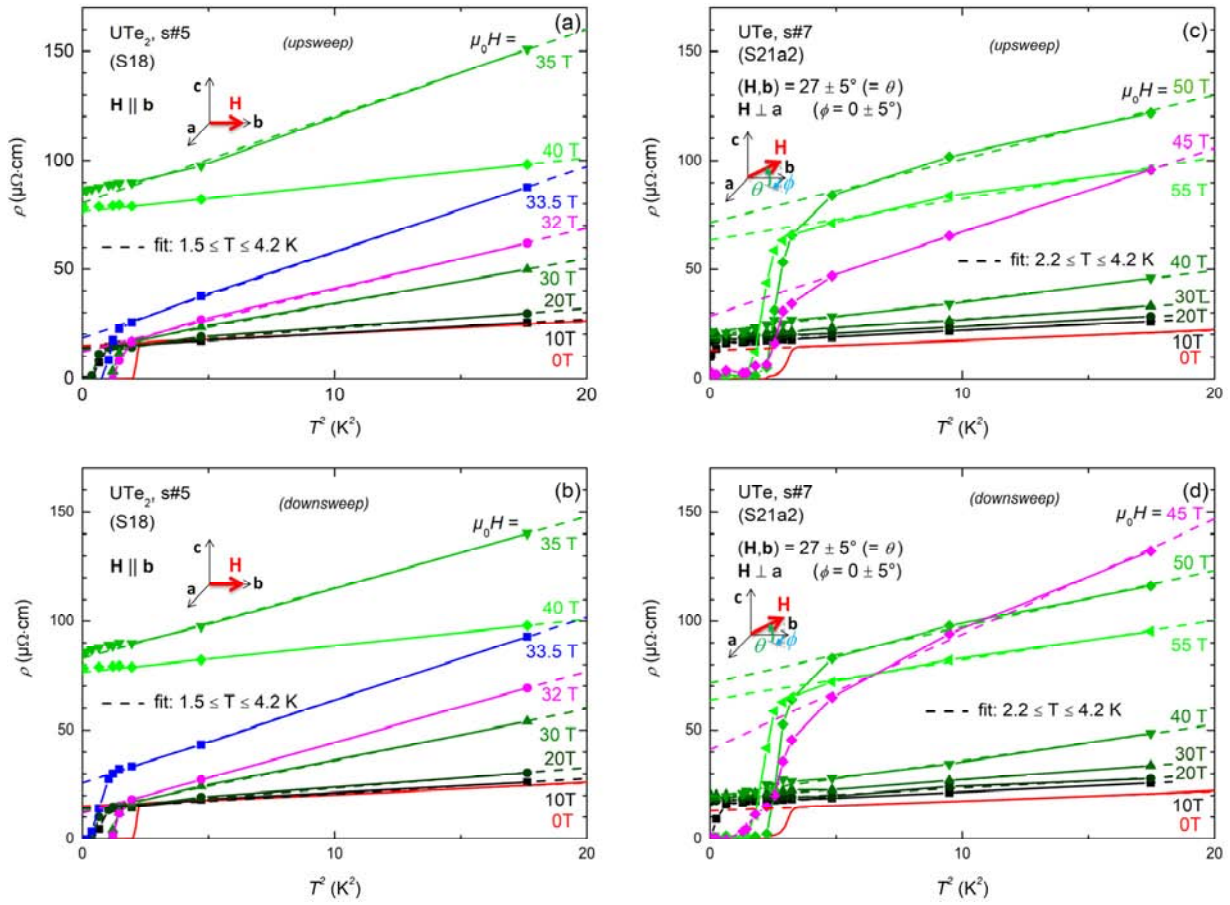
Supplementary Figure 4. Electrical resistivity of UTe₂ in a magnetic field H tilted by $27 \pm 5^\circ$ from b in the (b,c) plane. Comparison of field-up and field-down sweeps at temperatures from 1.5 K to 4.2 K.



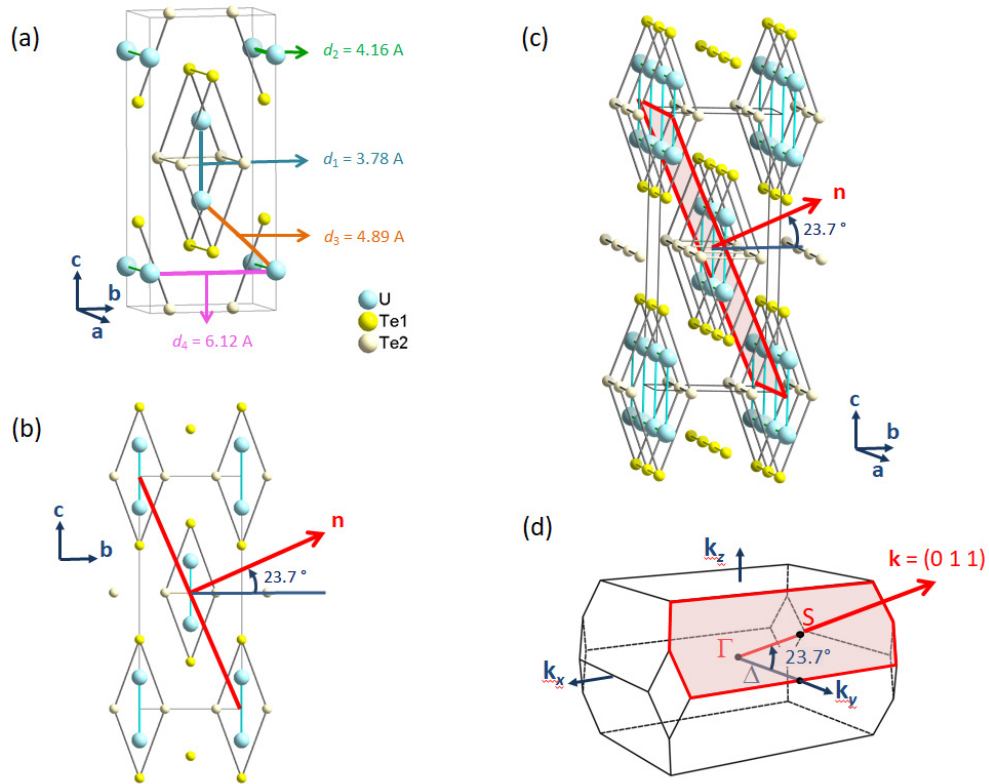
Supplementary Figure 5. Electrical resistivity of UTe_2 in the vicinity of the metamagnetic transition. (a) Low-temperature resistivity of UTe_2 in a magnetic field $H \parallel b$. (b) Low-temperature resistivity of UTe_2 in a magnetic field H tilted by $27 \pm 5^\circ$ from b in the (b,c) plane.



Supplementary Figure 6. Electrical resistivity of UTe_2 versus temperature in magnetic fields $H \parallel b$ and H tilted by $27 \pm 5^\circ$ from b in the (b,c) plane. Data are presented for field-up sweeps.



Supplementary Figure 7. Electrical resistivity of UTe_2 versus square of temperature and its T^2 fits in magnetic fields $H \parallel b$ and H tilted by $27 \pm 5^\circ$ from b in the (b, c) plane. Data are presented for field-up and field-down sweeps.



Supplementary Figure 8. Crystal structure and Brillouin zone of UTe_2 . (a) Elementary unit cell and identification of the four smallest U-U distances, (b) Projection of the lattice structure in the (b,c) plane, (c) Extended crystal structure emphasizing the network of two-leg ladders, and (d) Brillouin zone of UTe_2 . The vector \mathbf{n} normal to a family of reticular (and cleaving) planes of Miller indices $(0 \ 1 \ 1)$, with an angle $\theta = (\mathbf{b}, \mathbf{n}) = 23.7^\circ$, is indicated. These reticular planes are characteristic of the ladder structure. In the reciprocal space, the corresponding wavevector $\mathbf{k} = (0 \ 1 \ 1)$ is perpendicular to two planes of the Brillouin zone boundary.